Controlling bubble and skyrmion lattice order and dynamics via stripe domain engineering in ferrimagnetic Fe/Gd multilayers

Tim Titze, Sabri Koraltan, Timo Schmidt, Mailin Matthies, Amalio Fernández Pacheco, Dieter Suess, Manfred Albrecht, Stefan Mathias, Daniel Steil

Angaben zur Veröffentlichung / Publication details:

Titze, Tim, Sabri Koraltan, Timo Schmidt, Mailin Matthies, Amalio Fernández Pacheco, Dieter Suess, Manfred Albrecht, Stefan Mathias, and Daniel Steil. 2026. "Controlling bubble and skyrmion lattice order and dynamics via stripe domain engineering in ferrimagnetic Fe/Gd multilayers." *Advanced Physics Research* 5 (3): e00194. https://doi.org/10.1002/apxr.202500194.

Advanced Physics Research

ADVANCED PHYSICS RESEARCH Open Access

www.advphysicsres.com

RESEARCH ARTICLE OPEN ACCESS

Controlling Bubble and Skyrmion Lattice Order and Dynamics via Stripe Domain Engineering in Ferrimagnetic Fe/Gd Multilayers

Tim Titze[1] | Sabri Koraltan[3,4] | Timo Schmidt[5] | Mailin Matthies[1,2] | Amalio Fernández-Pacheco[4] | Dieter Suess[3] | Manfred Albrecht[5] | Stefan Mathias[1,2] | Daniel Steil[1]

[1]University of Göttingen, I. Physikalisches Institut, Göttingen, Germany | [2]University of Göttingen, International Center for Advanced Studies of Energy Conversion (ICASEC), Göttingen, Germany | [3]Physics of Functional Materials, Faculty of Physics, University of Vienna, Vienna, Austria | [4]Institute of Applied Physics, TU Wien, Vienna, Austria | [5]Institute of Physics, University of Augsburg, Augsburg, Germany

Correspondence: Daniel Steil (dsteil@gwdg.de)

Received: 24 October 2025 | **Revised:** 17 December 2025 | **Accepted:** 23 December 2025

Keywords: ferromagnetism | magnetic materials | skyrmions | topology | ultrafast magnetism

ABSTRACT

Ferrimagnetic Fe/Gd multilayers host maze-like stripe domains that transform into a disordered bubble/skyrmion lattice under out-of-plane magnetic fields at ambient temperature. Femtosecond magneto-optics distinguishes these textures via their distinct coherent breathing dynamics. Crucially, applying a brief in-plane "set" magnetic field to the stripe state enhances both frequency and amplitude of the bubble/skyrmion lattice breathing mode. Lorentz transmission electron microscopy, magnetic force microscopy, and micromagnetic simulations reveal that this enhancement arises from field-aligned stripes nucleating a dense, near-hexagonal bubble/skyrmion lattice upon out-of-plane field application, with strong indications for a pure skyrmion lattice. Thus, modifying the initial domain configuration by in-plane fields enables precise control of coherent magnetization dynamics on picosecond to nanosecond timescales and potentially even of topology.

1 | Introduction

Magnetic skyrmions, first observed in 2009 by Mühlbauer et al. [1], have attracted significant interest due to their tremendous potential in novel spintronic and magnonic devices [2–6]. One key reason is their intricate spin configuration, which gives rise to topological properties resulting in enhanced stability against perturbations. Magnetic skyrmions are commonly stabilized by the Dzyaloshinskii–Moriya interaction (DMI), either of interfacial [7–9] or bulk type [1, 10, 11]. However, they can also exist in multilayer thin films without DMI, where they are stabilized by the competition between dipolar interactions and perpendicular magnetic anisotropy [12–18]. In such dipolar-stabilized systems, no preferred chirality is imposed, allowing the coexistence of skyrmions of both helicities (type-1 bubbles, topological charge $Q = -1$) and topologically trivial type-2 bubbles (topological charge $Q = 0$). The ordering and density of these objects are of great interest for fundamental studies and future technological applications, e.g., in the context of magnonic crystals [19–21]. Achieving active control over their formation is therefore a key step toward unlocking the full potential of easy-to-grow, easily tunable multilayer thin films for skyrmion-based devices.

One particular system hosting mixed lattices of bubbles and skyrmions at ambient temperature are metallic ferrimagnetic Fe/Gd multilayers, which exhibit maze-like magnetic stripe domains transforming into a mixed bubble and skyrmion (BSK) lattice within a certain range of applied out-of-plane magnetic fields [16, 17, 22].

The different magnetic field–dependent spin textures in this system can, for example, be identified by observing the distinct coherent responses of the spin system following a femtosecond optical stimulus, a technique sucessfully applied previously for other systems as well [23–25]. This way, the stripe domain phases as well as BSK lattice states can be unequivocally distinguished in the time-domain without resorting to magnetic imaging methods [22]. Furthermore, strong optical excitation of the inherent magnetic spin textures allows for their nucleation or annihilation [22, 26], and even coherent control of the dynamics of BSK lattice states is possible using a double-pump excitation scheme [27].

Here, we showcase how controlling the initial stripe domain magnetic textures in Fe/Gd multilayers determines the density and ordering of the resulting cylindrical spin objects, achieving a highly dense, close to ideally ordered hexagonal BSK lattice. This effect is achieved by applying an in-plane magnetic set field to the sample prior to increasing the stabilizing out-of-plane magnetic field, which leads to a strongly enhanced coherent response in femtosecond magnetooptics and a large density of spin objects as observed in Lorentz transmission electron microscopy (LTEM), magnetic force microscopy (MFM), and supported by micromagnetic simulations. LTEM and micromagnetic simulations further indicate that this lattice is predominantly of skyrmion type, inferring the creation of a nearly perfect skyrmion lattice.

2 | Results

2.1 | Ground State Magnetic System Properties

Shortly summarizing our previous studies, see Refs. [22, 26], the studied Fe/Gd multilayers with composition $[\mathrm{Fe}(0.35\ \mathrm{nm})/\mathrm{Gd}(0.40\ \mathrm{nm})]_{160}$ show different kinds of spin textures under out-of-plane magnetic fields. Figure 1 displays the ground state magnetic spin textures stabilized at two exemplary magnetic fields ($\mu_0 H_{\mathrm{oop}} = 160$ mT and $\mu_0 H_{\mathrm{oop}} = 220$ mT). For the lower magnetic field, we find two distinct types of stripe domains, namely chiral and non-chiral stripe domains classified by the rotation sense of the magnetic moments across the domain walls [12]. Chiral stripe domains exhibit a full rotation of magnetic moments, either clockwise or counterclockwise, across both domain walls. In contrast, non-chiral stripe domains display opposite rotation senses at the two domain walls, i.e., they lack a defined chirality. These can be well distinguished in LTEM since non-chiral domain walls show a white-black contrast, while chiral domain walls exhibit a pronounced black-white-black or white-black-white contrast depending on their chirality, i.e., left- or right-handed rotation sense. When increasing the out-of-plane magnetic field, these stripe domains transform into cylindrical spin objects, namely topologically trivial bubbles as well as clockwise (CW) and counterclockwise (CCW) Bloch-type skyrmions. However, bubbles only emerge from non-chiral stripe domains, while skyrmions nucleate from chiral stripe domains with the corresponding chirality, meaning the chirality is preserved during the nucleation process. As shown in Ref. [26] and Figure S2a, such bubbles and skyrmions can be observed in an extended temperature region around ambient T.

2.2 | Magnetooptical Studies of Coherent Spin Dynamics

Following our recent works on detection of BSK lattices via femtosecond magnetooptics, Figure 2a depicts the laser-induced magnetization dynamics of the Fe/Gd multilayer system with composition $[\mathrm{Fe}(0.35\ \mathrm{nm})/\mathrm{Gd}(0.40\ \mathrm{nm})]_{160}$ in the weak perturbation limit, $F = 0.7$ mJ cm^{-2}. The data shown was recorded using an out-of-plane magnetic field $\mu_0 H_{\mathrm{oop}} = 196$ mT, i.e., in the BSK lattice state. Here, the blue transient shows the characteristic presence of the coherent BSK breathing mode [22, 26, 27] under application of only the out-of-plane magnetic field. Interestingly, application of an in-plane magnetic field $\mu_0 H_{\mathrm{ip}} = 149$ mT prior to the measurement significantly alters the observed dynamics, as depicted by the red transient. More specifically, we observe both an increase in amplitude and frequency of the breathing mode. Fourier analysis and fitting using a Gaussian error function reveals a frequency upshift of $\Delta f \approx 0.2$ GHz while increasing the in-plane magnetic field, see Figure 2b. In addition, we obtain a threshold in-plane magnetic field $\mu_0 H_{\mathrm{th,\,ip}} \approx 55$ mT that is required to drive the observed change in dynamics. This transition appears to be continuous, and in-plane magnetic fields $\mu_0 H_{\mathrm{ip}} \geqslant 100$ mT are required to achieve a full transformation.

This modification occurs solely due to the application of an in-plane magnetic field before the actual time-resolved measurements, suggesting that it arises from changes in the underlying static magnetic spin textures of the system. Therefore, we now compare the two different pathways induced by the initial magnetic domain configuration, which can be tailored by applying in-plane magnetic set fields. The resulting spin textures in out-of-plane magnetic fields are analyzed by LTEM, MFM, and micromagnetic simulations.

2.3 | Imaging of Magnetic Spin Textures

Figure 3a shows the magnetic spin textures obtained from LTEM, MFM, and micromagnetic simulations by applying only an out-of-plane magnetic field. Note that the LTEM images were obtained from a $[\mathrm{Fe}(0.35\ \mathrm{nm})/\mathrm{Gd}(0.42\ \mathrm{nm})]_{120}$ multilayer sample on a 30 nm thick Si_3N_4 membrane, which has somewhat different magnetic properties than the rigid thin film in MOKE experiments due to membrane buckling effects (see Supporting Information). In contrast, the MFM data was taken from a piece of the $[\mathrm{Fe}(0.35\ \mathrm{nm})/\mathrm{Gd}(0.40\ \mathrm{nm})]_{160}$ sample studied in the time-resolved measurements. Therefore, LTEM data, which allows to clearly distinguish chiral and non-chiral stripe domains, as well as bubbles and skyrmions, is used for purely qualitative understanding of spin texture changes due to additional in-plane fields, whereas MFM data is used for quantitative understanding of field-induced changes. A comparison of the very similar magnetic hysteresis loops of both samples, as measured by superconducting quantum interference device (SQUID) magnetometry, can be found in the Supporting Information. By increasing the out-of-plane magnetic field from $\mu_0 H_{\mathrm{oop}} = 0$ mT up to $\mu m_0 H_{\mathrm{oop}} = 290$ mT, the magnetic spin textures change from a maze-like stripe domain state into a mixed state of stripe domains and cylindrical spin objects, and finally into a disordered BSK lattice, before the single domain state is formed. In more detail, micromagnetic simulations predict a mixed lattice of bubbles and skyrmions with

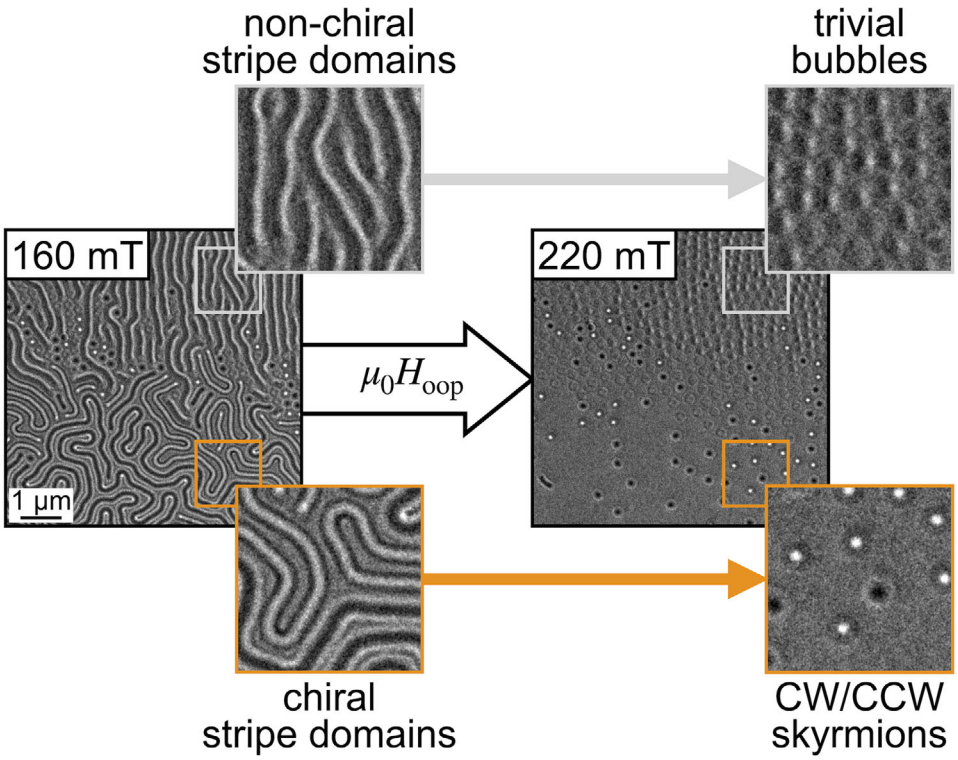

FIGURE 1 | Ground state magnetic spin textures hosted by the $[Fe(0.35\ nm)/Gd(0.42\ nm)]_{120}$ multilayer film for LTEM studies. At low magnetic fields, the system exhibits two distinct types of stripe domains: chiral and non-chiral stripe domains. At high out-of-plane magnetic fields, the chiral stripe domains have been transformed into clockwise (CW) and counterclockwise (CCW) skyrmions (orange), while topologically trivial bubbles have emerged from the non-chiral ones (gray).

a density of 4.4 μm^{-2} at $\mu_0 H_{oop} = 220$ mT, lower than the density of cylindrical spin objects observed for the rigid thin film sample in MFM, which is 7.5 μm^{-2}. LTEM data, in contrast, shows only a low number, respectively density of purely skyrmionic objects in the depicted field of view (FOV). We note that the density and type of spin objects in LTEM strongly depends on the aforementioned membrane buckling, which is expected to be minimized in the given FOV. Thereby, considering magnetic properties, this FOV should correspond best to the thin film on the rigid Si substrate used in MFM and optical measurements, even though the total number of skyrmions is low. In regions that exhibit stronger membrane buckling, both bubbles and skyrmions are present as shown in Figure 1 and Figure S3. Furthermore, their density does not significantly change with applying an external in-plane field, because the additional in-plane component of the out-of-plane field present due to the buckling already pre-aligns stripe domains, as highlighted in Figure S3.

Figure 3b now shows snapshots of the magnetic spin textures for the same out-of-plane magnetic fields, but before increasing the out-of-plane magnetic field from zero to saturation, an in-plane magnetic set field was temporarily applied. The effect of an applied in-plane field of $\mu_0 H_{ip} = 50$ mT at zero out-of-plane magnetic field in the micromagnetic simulation is an alignment of the initial maze-like stripe domains, now forming Bloch-type domain walls parallel to the in-plane field. Turning this field off preserves the parallel domain wall alignment. Gradually increasing the external out-of-plane magnetic field in the simulation to $\mu_0 H_{oop} = 220$ mT, once again transforms oriented stripes into a mixed BSK lattice with an initially large number of bubbles, see also Figure S4. Intriguingly, skyrmions nucleate despite the stripe domains lacking chirality. In addition, the resulting lattice exhibits an about 20% higher density (5.2 μm^{-2}) at $\mu_0 H_{oop} = 220$ mT than in the previous case (4.4 μm^{-2}) and an ordering, which is now closer to an ideal hexagonal lattice structure. Further increase of the magnetic field yields a single skyrmion lattice (see also Figure S4), i.e., the initially created bubbles appear to be extremely unstable. A similar transitional bubble state in a stripe domain to skyrmion transformation under the influence of an additional in-plane magnetic field was recently discussed in Ref. [28] for Néel-type skyrmions stabilized by DMI, also leading to a single skyrmion lattice with enhanced density.

The findings in the simulation are in very good agreement with the results obtained from LTEM, which also showcase the alignment of the domain walls by the in-plane field. In LTEM, the application of an aligning in-plane field is achieved by tilting the sample by 30° in an applied out-of-plane field prior to the application of the actual out-of-plane field at zero tilt angle (for details see Experimental section). However, in contrast to the micromagnetic simulations, non-chiral stripe domains seem to directly transform into a single skyrmion lattice upon increasing the out-of-plane magnetic field. An intermediate bubble state may not be observable if the bubbles are comparably unstable as those in the simulation. Interestingly, the number of skyrmions at $\mu_0 H_{oop} = 220$ mT within the same FOV is now massively increased compared to Figure 3a, forming a dense, close to hexagonal lattice with a density of 7.7 μm^{-2}.

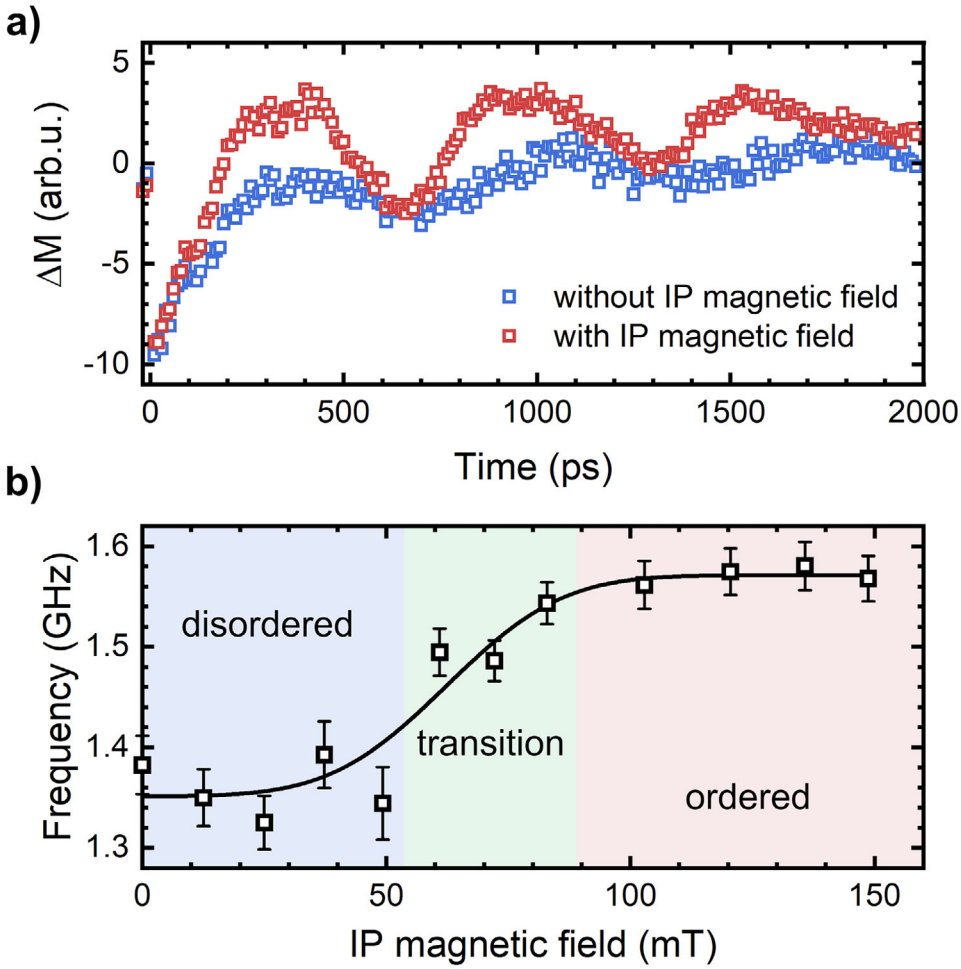

FIGURE 2 | The effect of initial in-plane magnetic set fields on the coherent magnetization dynamics. (a) Laser-induced magnetization dynamics using an out-of-plane magnetic field $\mu_0 H_{oop} = 196$ mT. In the case of the red squares, an in-plane magnetic set field $\mu_0 H_{ip} = 149$ mT was switched on prior to the measurement to align the demagnetized stripe domain state. (b) Fourier analysis of the breathing mode frequency for various in-plane magnetic set fields, which were applied prior to the constant out-of-plane magnetic field $\mu_0 H_{oop} = 196$ mT.

The increase in the density of cylindrical spin objects is as well corroborated by the MFM measurements on the sample on the rigid substrate. Here, application of an in-plane field prior to the out-of-plane field again shows the alignment of maze-like stripe domains and the resulting density of spin objects at $\mu_0 H_{oop} = 220$ mT is 11.4 μm^{-2} compared to 7.5 μm^{-2} without application of the in-plane field, an increase of about 50%.

In total, LTEM, MFM, and micromagnetic simulations all show that briefly applying an in-plane magnetic set field at zero out-of-plane field leads to an alignment of maze-like stripe domains, and that application of a large enough out-of-plane field transforms these stripe domains into a lattice of cylindrical spin objects with increased density compared to the case without in-plane field. Furthermore, micromagnetic simulations and LTEM indicate that such a procedure may lead to the formation of a pure skyrmion lattice, as bubbles created this way seem to be very unstable in magnetic fields, see Figure S4.

2.4 | Dynamical Response to Laser Excitation in Micromagnetic Simulations

How do these observations now relate to the observed changes in both breathing mode amplitude and frequency in the MOKE experiment? To elucidate the origin of these changes, we employed dynamic micromagnetic simulations modeling the laser-induced breathing mode dynamics, following the approach of our recent studies [22, 27]. Figure 4a,b displays these coherent magnetization dynamics resulting from excitation of an initial state without and with prior in-plane magnetic set field. Furthermore, we compare the dynamics obtained from a single excitation and after eight excitations, i.e., following consecutive simulated laser excitations. While the dynamics only slightly differ in case of no applied in-plane magnetic field, there is a significant change in both frequency and amplitude when an in-plane magnetic set field is used to modify the initial state. Furthermore, comparing the eighth excitation of both cases, we find an increased frequency ($\Delta f \approx 0.05$ GHz) and amplitude when applying the in-plane magnetic field, qualitatively similar to the experiment.

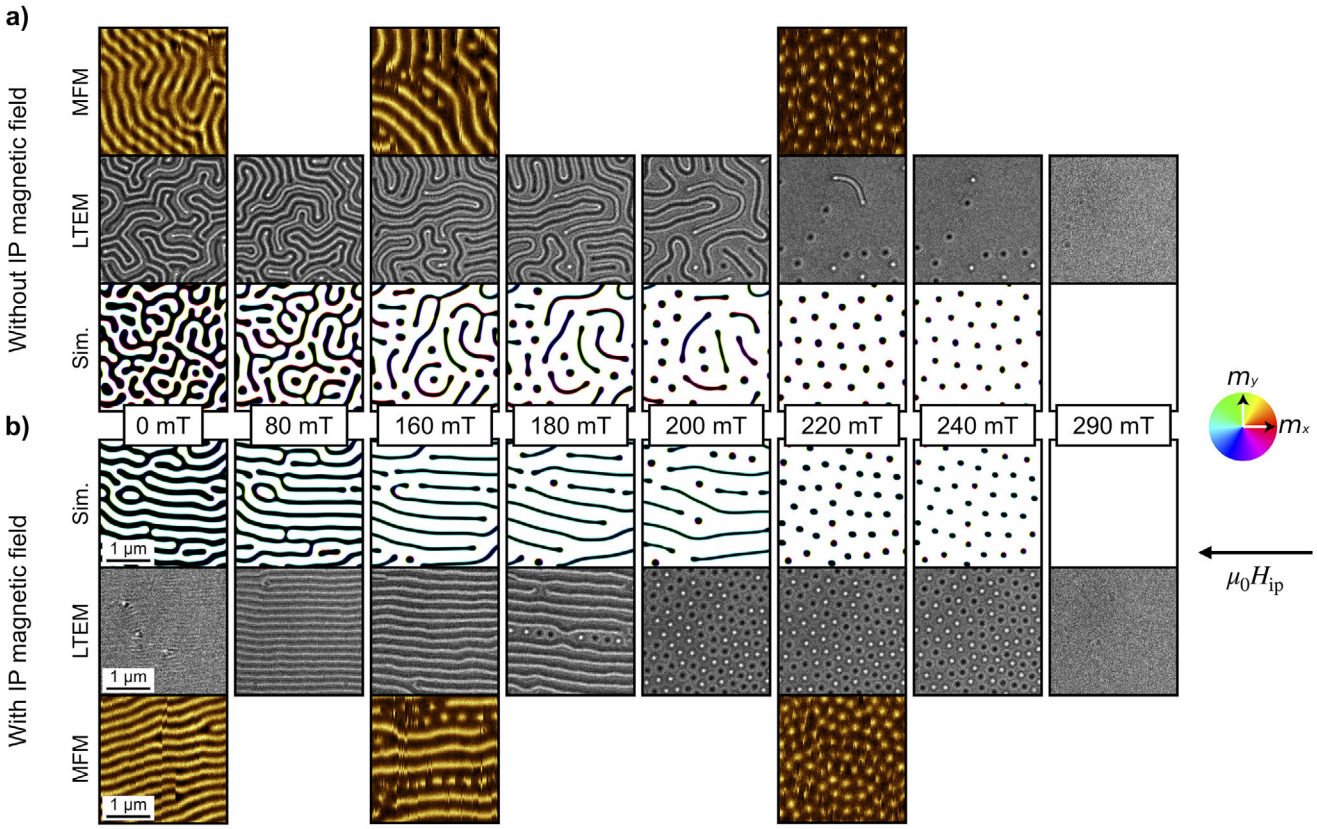

FIGURE 3 | The effect of in-plane magnetic set fields on the magnetic spin textures. (a) Magnetic spin textures obtained from micromagnetic simulations, LTEM, and MFM considering various out-of-plane magnetic fields as given in the center of the image. (b) An in-plane magnetic set field was applied prior to increasing the out-of-plane magnetic field to align the stripe domain state. For the region shown in the LTEM images, which is approximately the same for all images, membrane buckling effects are minimized. The LTEM measurements were carried out on a $[Fe(0.35\ nm)/Gd(0.42\ nm)]_{120}$ sample, while the MFM measurements and micromagnetic simulations were performed on the $[Fe(0.35\ nm)/Gd(0.40\ nm)]_{160}$ sample, which was used for the optical experiments.

The micromagnetic simulations allow us to explore the reason for these observed changes. The prior application of an in-plane magnetic set field modifies the initial state in a way that more topologically trivial bubbles are stabilized and the overall density of spin objects is increased by about 20%, see also Figure 3. However, almost all of these bubbles are transformed into non-trivial skyrmions upon consecutive laser excitation, see Figure 5. This is the reason for the increase in frequency and amplitude of the breathing mode that we observe after eight laser excitations in the simulation, as skyrmions show a faster and more pronounced expansion and contraction of their core size than bubbles [22]. Comparing the two cases with and without in-plane magnetic set field after eight excitations, the in-plane field treatment results in an additional increase of breathing frequency and amplitude. This can be unequivocally related to the 20% enhanced density of spin objects as almost no bubbles remain after multiple excitations, i.e., the observed breathing mode predominantly originates from skyrmions in both cases. We note that the observed increase in frequency, and particularly in amplitude, is rather weak compared to the experimental data shown in Figure 2a. We relate this effect to the relatively small increase in spin object density in the simulation in contrast to the experiment (see MFM data in Figure 3).

Going into more detail, the aforementioned transformation of topologically trivial bubbles into non-trivial skyrmions upon laser excitation is displayed in Figure 5. We start with an initial state shown in Figure 5a, which is created by briefly applying an in-plane magnetic set field $\mu_0 H_{ip} = 50$ mT before increasing the out-of-plane magnetic field to $\mu_0 H_{oop} = 220$ mT. Laser excitation then yields the transformation of bubbles to skyrmions as evident from the snapshot at 2 ns after excitation. We further examine the transformation process in Figure 5b by monitoring the evolution of the 3D structure of the in-plane magnetic moments across the film thickness. The upper panel displays a bubble, which is not transformed upon laser excitation. In contrast, the lower panel shows a bubble that is transformed into a skyrmion. This transformation process is mediated by the formation of a Bloch point, a topological magnetic singularity [29–32], at approximately 0.5 ns after laser excitation and it is fully completed after 1.5 ns. We suggest that the laser-induced transformation of bubbles is only possible because they resemble a metastable state in this system, as also pointed out by Jefremovas et al. [28]. Under real experimental conditions, bubbles can therefore not be stabilized on observable timescales, as highlighted by the LTEM measurements shown in Figure 3.

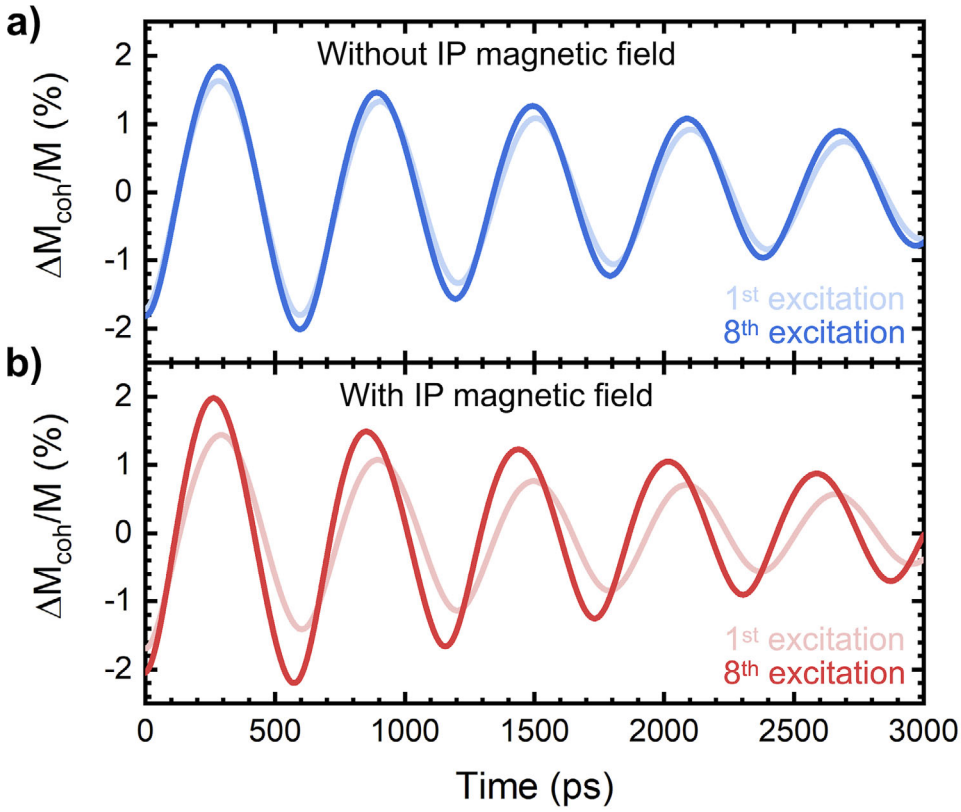

FIGURE 4 | Coherent magnetization dynamics obtained from micromagnetic simulations. (a) Coherent magnetization dynamics after 1 and 8 excitations of the initial state created without applying an in-plane magnetic field, and (b) of the initial state for which an in-plane magnetic set field has been applied prior to increasing the out-of-plane magnetic field.

3 | Discussion

Combining the experimental results and micromagnetic simulations, we now explain the changes in the experimentally observed breathing mode amplitude and frequencies in Figure 2. In agreement with LTEM, MFM, and micromagnetic simulations, as well as Refs. [28, 33], applying an in-plane magnetic field significantly increases the density of spin objects, here by about 50% according to the MFM data. We attribute this to a unique mechanism of skyrmion nucleation from non-chiral stripe domains, leading to a pure, close to hexagonally ordered skyrmion lattice state. This skyrmion lattice emerges from an ordered, but metastable bubble lattice state after the formation of Bloch points. These Bloch points appear in the micromagnetic simulations at about 0.5 ns after weak laser excitation, presumably in response to the laser-induced disturbance of the system magnetization as the system recovers to a more stable state configuration.

The higher density of spin objects gives rise to an enhanced frequency and amplitude of the breathing mode in the femtosecond experiment, as corroborated by dynamic micromagnetic simulations [1]. The amplitude increases, since more spin objects contribute to the collective breathing mode. However, the higher density of spin objects also results in a reduced distance between neighboring spin objects. This in turn induces stronger repulsive forces [34, 35], which give rise to the observed higher breathing mode frequency. Furthermore, not only the amplitude and frequency of the breathing mode are increased, but also the equilibrium position of oscillation is shifted. In Figure 2a the minima, at which the spin objects reach their maximum size, almost overlap, while the maxima, indicating the minimum size of the spin objects, are clearly separated. In other words, the maximum size of the spin objects during the breathing mode oscillation is limited, which we attribute to the collective expansion and contraction of the individual spin objects within the dense, ordered lattice structure. In fact, the closely packed lattice prohibits further expansion of the spin objects as they feel their corresponding neighbors, an effect most likely not relevant in the simulation due to the less dense skyrmion packing.

4 | Conclusion

In summary, we found that applying an in-plane magnetic set field prior to establishing a specific out-of-plane magnetic field in Fe/Gd multilayer films modifies both the amplitude and frequency of laser-induced breathing modes. Using LTEM, MFM, and micromagnetic simulations, we explained the observed changes by a persistent modification of the ground state magnetic spin textures by the in-plane magnetic set field, allowing for the creation of a larger amount of spin objects within the BSK lattice structure. In more detail, our studies indicate the formation of a more dense, hexagonally ordered single skyrmion lattice. Other approaches for controlling the nucleation sites or density of skyrmionic objects typically rely on modifying the magnetic anisotropy permanently, e.g., via local ion irradiation, as shown in [36]. The larger breathing amplitude we observe follows from the enhanced density of spin objects, since more

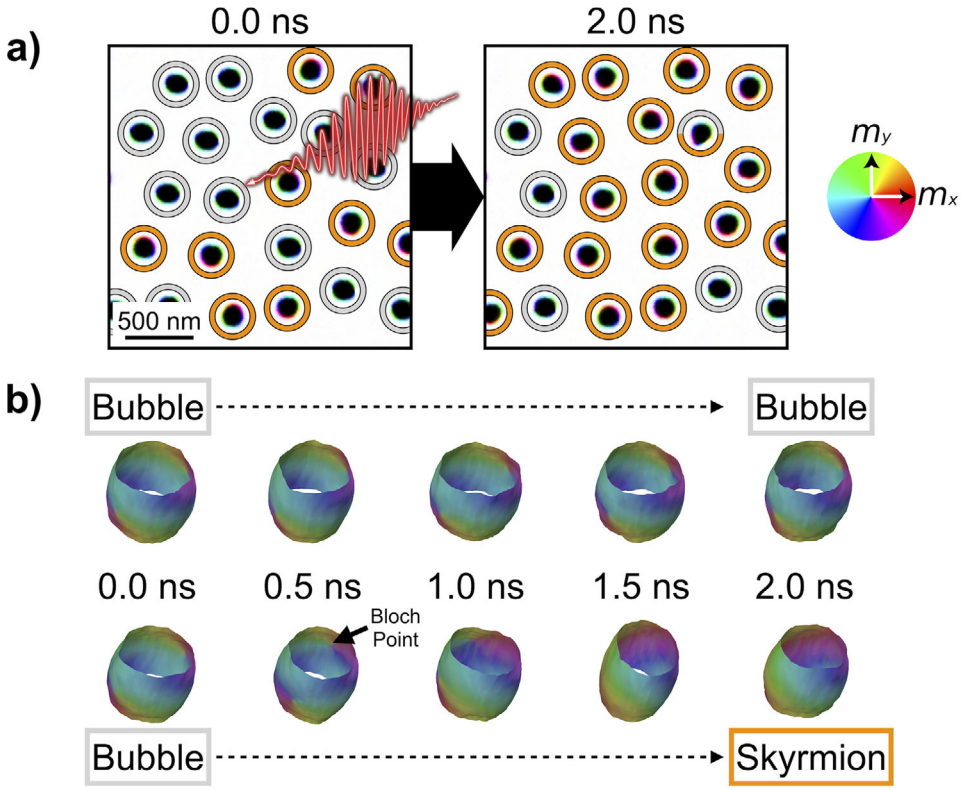

FIGURE 5 | Transformation of topologically trivial bubbles into non-trivial skyrmions. (a) The initial state in the simulation is created by briefly applying an in-plane magnetic set field of $\mu_0 H_{ip} = 50$ mT before increasing the out-of-plane magnetic field to $\mu_0 H_{oop} = 220$ mT. Most of the topologically trivial bubbles (highlighted by gray circles) transform into non-trivial skyrmions (orange circles) upon laser excitation. (b) 3D representation of two topologically trivial bubbles. While the bubble in the upper panel remains unchanged, the bubble in the lower panel transforms into a non-trivial skyrmion by introducing a Bloch point at around 0.5 ns after laser excitation. The transformation process is completed at approximately 1.5 ns.

objects contribute to the collective breathing mode. Similarly, the experimentally observed higher frequency can be related to increased repulsive forces between neighboring objects due to their reduced distance. The shift in the equilibrium position of the breathing may be indicative of the relevance of interactions between the different spin objects, limiting their maximum expansion within the lattice. In total, our observations show a pathway for actively controlling and harnessing the density and ordering of dipolar-stabilized spin objects in multilayer thin films, potentially allowing even for topology control, which might be of interest for future applications.

5 | Experimental Section

5.1 | Time-Resolved Magneto-Optical Kerr Effect (TR-MOKE)

Magnetization dynamics $\Delta M(t)$ of a $[\mathrm{Fe}(0.35\,\mathrm{nm})/\mathrm{Gd}(0.40\,\mathrm{nm})]_{160}$ thin film, deposited onto a thermally-oxidized Si(100) substrate, were measured using a bichromatic pump-probe setup. Sub-ps laser pulses at a repetition rate of 50 kHz were provided by a fiber amplifier system. These pulses were compressed to less than 40 fs using spectral broadening in a gas-filled hollow core fiber and compression by chirped mirrors. The fundamental light pulses with a central wavelength of 1030 nm were used as pump pulses, while their second harmonic at 515 nm represent the probe pulses. External out-of-plane magnetic fields up to $\mu_0 H_{oop} = 0.5$ T could be applied in-between the poles of a variable-gap electromagnet. There, we added another electromagnet with a fixed gap to provide an external in-plane magnetic field of up to $\mu_0 H_{ip} = 0.2$ T at the centered sample position. A balanced bridge detector was used to measure laser-induced polarization changes, which can be related to magnetization changes. The data was acquired by a 250 MHz digitzer card in a chopped measurement mode, allowing for maximum scope of data post processing. Note that the setup makes use of a stroboscopic pump-probe method, i.e., only reversible dynamics are accessible, and one data point for a given time-delay and set out-of-plane magnetic field represents the average signal over thousands of pump-probe cycles.

5.2 | Micromagnetic Simulations

We used `magnum.np` [37] to perform micromagnetic simulations using the finite-difference method. The simulations were carried out on the $[\mathrm{Fe}(0.35\,\mathrm{nm})/\mathrm{Gd}(0.40\,\mathrm{nm})]_{160}$ sample using a box of dimensions $(512 \times 512 \times 10)$ where each cell had the size $(10 \times 10 \times 12\,\mathrm{nm}^3)$. 2D periodic boundary conditions were used with 10 repetitions in each direction. The material parameters at $T = 300$ K are: $M_s = 340\mathrm{kA\,m^{-1}}$, $K_u = 40\,\mathrm{kJ\,m^{-3}}$ and $A = 6\,\mathrm{pJ\,m^{-1}}$,

which have yielded excellent agreement with experiments in the past [26, 27].

5.2.1 | Static Simulations

We start from a random magnetization state, selected by a manual seed, and proceed with the following simulation protocol. First, we relax the magnetization at vanishing magnetic fields by numerically integrating the Landau–Lifshitz–Gilbert (LLG) equation for 5 ns by considering the contributions from demagnetization, exchange and anisotropy energies. Thermal fluctuations are neglected at this state. Then, an in-plane magnetic field is applied ($\mu_0 H_{ip}$ = 25–100 mT), and the magnetic configuration is relaxed with the additional Zeeman energy. In a third step, the magnetization is relaxed at vanishing fields. From here on, we include a time-dependent external out-of-plane magnetic field into the energy terms, where the $\mu_0 H_z$ component of the field increases from 0 to 300 mT in 6 µs. The magnetization state is then recorded every 10 ns.

5.2.2 | Dynamic Simulations

We follow closely the approach adapted in Ref. [27], where an effective temperature is calculated from the time-dependent change in total magnetization, which was recorded experimentally. We choose $\mu_0 H_z$ = 220 mT, and α = 0.02. The initial magnetic state is obtained from the static simulations described above. Thermal fluctuations are now considered [37]. First, the magnetization is relaxed under the consideration of the thermal fluctuations at T = 300 T. Then, the laser-excitation is mimicked by following the experimental demagnetization curve. The magnetization is recorded for 3 ns, until an equilibrium state is reached. The excitation scheme is repeated 8 times, to investigate the influence of the stroboscopic measurement technique employed in the experiments.

5.3 | Lorentz Transmission Electron Microscopy

The LTEM imaging of the magnetic spin structure in the thin films deposited on the membranes was realized using a JEOL NEOARM-200F TEM system in Fresnel mode. A tilting holder was used in order to change the angle between the sample surface and the applied magnetic field. We employed the following experimental procedure. First, the disordered stripe state was set in the sample by an out-of-plane demagnetization routine. We then imaged the magnetic states at increasing applied out-of-plane fields. After the sample reached the saturated state, the experiment was reset by returning to zero-field. Now, the aligned stripe state was set by tilting the sample by 30° with respect to the original sample surface orientation and applying a moderate field, which now entails a considerable in-plane component. After returning to zero-field and zero-tilt, we then imaged the following evolution of the magnetic state by increasing the applied magnetic field. With this protocol, the evolution of both states could be imaged for the same membrane area, which was chosen due to low membrane buckling effects and mostly planar arrangement.

5.4 | Magnetic Force Microscopy

A Bruker Dimension Icon System was used to perform MFM Imaging employing low-moment tips. The applied magnetic field was realized by placing a permanent magnet (N45) and spacers beneath the sample during scanning. Prior to the scans with an applied field, appropriate amounts of spacers were placed between the permanent magnet and the sample and the field strengths at the position of the scan were measured with a Hall sensor. This way, two setups were found for 160 and 220 mT, corresponding to the mixed state of stripe domains and cylindrical spin objects, and a BSK lattice, respectively. In order to set the disordered stripe state in the sample, analogously to the LTEM experiment, an out-of-plane demagnetization routine was applied to the $[Fe(0.35\,nm)/Gd(0.40\,nm)]_{160}$-film on a rigid silicon substrate. The aligned stripe state was set by applying an in-plane field to the sample with a permanent magnet in its proximity. Prior to every scan the desired magnetic state was set, and the sample was placed onto the magnet and spaceholders to apply the field.

Author Contributions

S. Mathias and D. Steil conceived the project. T. Titze and M. Matthies performed the time-resolved Kerr effect studies and analyzed the time-resolved magnetization data under the supervision of S. Mathias and D. Steil. Sample growth, MFM measurements, and LTEM measurements were performed by T. Schmidt under the supervision of M. Albrecht. S. Koraltan performed the micromagnetic simulations under the supervision of D. Suess and A. Fernández–Pacheco. The simulations were evaluated by S. Koraltan and T. Titze with support from D. Steil. T. Titze and D. Steil wrote the manuscript with input from all authors.

Acknowledgments

T.T. and D.S. gratefully acknowledge funding by the Deutsche Forschungsgemeinschaft (DFG, German Research Foundation), Grant No. 217133147 (SFB1073, project A02). T.S. and M.A. gratefully acknowledge funding by the Deutsche Forschungsgemeinschaft (DFG, German Research Foundation) Grant No. 507821284 and 540566574. S.K. and D.Su. acknowledge the Austrian Science Fund (FWF) for support through Grant No. I 6267 (CHIRALSPIN). S.K. , and A.F.P. acknowledge funding from the European Research Council (ERC) under the European Union's Horizon 2020 research and innovation programme, Grant Agreement No. 101001290 (3DNANOMAG). We acknowledge Vienna Scientific Cluster (VSC) for awarding this project access to the LEONARDO supercomputer, owned by the EuroHPC Joint Undertaking, hosted by CINECA (Italy) and the LEONARDO consortium.

We acknowledge support by the Open Access Publication Funds of the Göttingen University via Project DEAL.

Conflicts of Interest

The authors declare no conflicts of interest.

Data Availability Statement

The data that support the findings of this study are available from the authors upon reasonable request. The data that support the findings of this study are available from the corresponding author upon reasonable request.

Endnotes

[1] Note that these changes are considerably smaller than those observed experimentally, which is related to the smaller changes in density in the simulation compared to the MFM.

References

1. S. Mühlbauer, B. Binz, F. Jonietz, et al., "Skyrmion Lattice in a Chiral Magnet," *Science* 323, no. 5916 (2009): 915–919.

2. N. Nagaosa and Y. Tokura, "Topological Properties and Dynamics of Magnetic Skyrmions," *Nature Nanotechnology* 8, no. 12 (2013): 899–911.

3. G. Finocchio, F. Büttner, R. Tomasello, M. Carpentieri, and M. Kläui, "Magnetic Skyrmions: From Fundamental to Applications," *Journal of Physics D: Applied Physics* 49, no. 42 (2016): 423001.

4. A. Fert, N. Reyren, and V. Cros, "Magnetic Skyrmions: Advances in Physics and Potential Applications," *Nature Reviews Materials* 2, no. 7 (2017): 1–15.

5. J. Grollier, D. Querlioz, K. Y. Camsari, K. Everschor-Sitte, S. Fukami, and M. D. Stiles, "Neuromorphic Spintronics," *Nature Electronics* 3, no. 7 (2020): 360–370.

6. H. Yu, J. Xiao, and H. Schultheiss, "Magnetic Texture Based Magnonics," *Physics Reports* 905 (2021): 1–59.

7. S. Heinze, K. von Bergmann, M. Menzel, et al., "Spontaneous Atomic-Scale Magnetic Skyrmion Lattice in Two Dimensions," *Nature Physics* 7, no. 9 (2011): 713–718.

8. G. Chen, A. Mascaraque, A. T. N'Diaye, and A. K. Schmid, "Room Temperature Skyrmion Ground State Stabilized Through Interlayer Exchange Coupling," *Applied Physics Letters* 106, no. 24 (2015): 242404.

9. S. Woo, K. Litzius, B. Krüger, et al., "Observation of Room-Temperature Magnetic Skyrmions and Their Current-Driven Dynamics in Ultrathin Metallic Ferromagnets," *Nature Materials* 15, no. 5 (2016): 501–506.

10. W. Münzer, A. Neubauer, T. Adams, et al., "Skyrmion Lattice in the Doped Semiconductor $Fe_{1-x}Co_xSi$," *Physical Review B* 81 (2010): 041203.

11. X. Z. Yu, Y. Onose, N. Kanazawa, et al., "Real-Space Observation of a Two-Dimensional Skyrmion Crystal," *Nature* 465, no. 7300 (2010): 901–904.

12. X. Yu, M. Mostovoy, Y. Tokunaga, et al., "Magnetic Stripes and Skyrmions With Helicity Reversals," *Proceedings of the National Academy of Sciences* 109, no. 23 (2012): 8856–8860.

13. J. C. T. Lee, J. J. Chess, S. A. Montoya, et al., "Synthesizing Skyrmion Bound Pairs in Fe-Gd Thin Films," *Applied Physics Letters* 109, no. 2 (2016): 022402.

14. R. D. Desautels, L. DeBeer-Schmitt, S. A. Montoya, et al., "Realization of Ordered Magnetic Skyrmions in Thin Films at Ambient Conditions," *Physical Review Materials* 3 (Oct 2019): 104406.

15. J. Zhang, X. Zhang, H. Chen, et al., "Formation and Magnetic-Field Stability of Magnetic Dipole Skyrmions and Bubbles in a Ferrimagnet," *Applied Physics Letters* 116, no. 14 (2020): 142404.

16. S. A. Montoya, S. Couture, J. J. Chess, et al., "Tailoring Magnetic Energies to Form Dipole Skyrmions and Skyrmion Lattices," *Physical Review B* 95 (2017): 024415.

17. M. Heigl, S. Koraltan, M. Vaňatka, et al., "Dipolar-Stabilized First- and Second-Order Antiskyrmions in Ferrimagnetic Multilayers," *Nature Communications* 12 (2021): 2611.

18. M. Hassan, S. Koraltan, A. Ullrich, et al., "Dipolar Skyrmions and Antiskyrmions of Arbitrary Topological Charge at Room Temperature," *Nature Physics* 20, no. 4 (2024): 615–622.

19. A. V. Chumak, A. A. Serga, and B. Hillebrands, "Magnonic Crystals for Data Processing," *Journal of Physics D: Applied Physics* 50, no. 24 (2017): 244001.

20. M. Lonsky and A. Hoffmann, "Dynamic Excitations of Chiral Magnetic Textures," *APL Materials* 8, no. 10 (2020): 100903.

21. Z. Chen and F. Ma, "Skyrmion Based Magnonic Crystals," *Journal of Applied Physics* 130, no. 9 (2021): 090901.

22. T. Titze, S. Koraltan, T. Schmidt, et al., "Laser-Induced Real-Space Topology Control of Spin Wave Resonances," *Advanced Functional Materials* 34 (2024): 2313619.

23. N. Ogawa, S. Seki, and Y. Tokura, "Ultrafast Optical Excitation of Magnetic Skyrmions," *Scientific Reports* 5, no. 1 (2015): 9552.

24. P. Padmanabhan, F. Sekiguchi, R. B. Versteeg, et al., "Optically Driven Collective Spin Excitations and Magnetization Dynamics in the Néel-Type Skyrmion Host GaV_4S_8," *Physical Review Letters* 122 (2019): 107203.

25. J. Kalin, S. Sievers, H. Füser, et al., "Optically Excited Spin Dynamics of Thermally Metastable Skyrmions in $Fe_{0.75}Co_{0.25}$," *Physical Review B* 106 (2022): 054430.

26. T. Titze, S. Koraltan, M. Matthies, et al., "Pathways to Bubble and Skyrmion Lattice Formation in Fe/Gd Multilayers," *Physical Review B* 112 (2025): 064413.

27. T. Titze, S. Koraltan, T. Schmidt, et al., "All-Optical Control of Bubble and Skyrmion Breathing," *Physical Review Letters* 133 (2024): 156701.

28. E. M. Jefremovas, K. Leutner, M. G. Fischer, et al., "The Role of Magnetic Dipolar Interactions in Skyrmion Lattices," *Newton* 1, no. 2 (2025): 100036.

29. A. Kosevich, B. Ivanov, and A. Kovalev, "Magnetic Solitons," *Physics Reports* 194, no. 3 (1990): 117–238.

30. A. Hierro-Rodriguez, C. Quirós, A. Sorrentino, et al., "Revealing 3D Magnetization of Thin Films With Soft X-Ray Tomography: Magnetic Singularities and Topological Charges," *Nature Communications* 11, no. 1 (2020): 6382.

31. F. Tejo, R. H. Heredero, O. Chubykalo-Fesenko, and K. Y. Guslienko, "The Bloch Point 3D Topological Charge Induced by the Magnetostatic Interaction," *Scientific Reports* 11, no. 1 (2021): 21714.

32. B. Göbel, I. Mertig, and O. A. Tretiakov, "Beyond Skyrmions: Review and Perspectives of Alternative Magnetic Quasiparticles," *Physics Reports* 895 (2021): 1–28.

33. S. Zhang, J. Zhang, Y. Wen, E. M. Chudnovsky, and X. Zhang, "Determination of Chirality and Density Control of Néel-Type Skyrmions With In-Plane Magnetic Field," *Communications Physics* 1, no. 1 (2018): 36.

34. X. Zhang, G. P. Zhao, H. Fangohr, et al., "Skyrmion-Skyrmion and Skyrmion-Edge Repulsions in Skyrmion-Based Racetrack Memory," *Scientific Reports* 5, no. 1 (2015): 7643.

35. M. A. Castro, D. Mancilla-Almonacid, J. A. Valdivia, and S. Allende, "Magnetostatic Interaction Between Two Bubble Skyrmions," *Journal of Physics: Condensed Matter* 32, no. 17 (2020): 175801.

36. L.-M. Kern, V. M. Kuchkin, V. Deinhart, et al., "Controlled Formation of Skyrmion Bags," *Advanced Materials* 37, no. 29 (2025): 2501250.

37. F. Bruckner, S. Koraltan, C. Abert, and D. Suess, "Magnum.np: A PyTorch Based GPU Enhanced Finite Difference Micromagnetic Simulation Framework for High-Level Development and Inverse Design," *Scientific Reports* 13, no. 1 (2023): 12054.

Supporting Information

Additional supporting information can be found online in the Supporting Information section.

Supporting File: apxr70076-sup-0001-SuppMat.pdf.